A meshless sub-region radial point interpolation method for accurate calculation of crack tip fields

Xiaoying Zhuang [a,c], Yongchang Cai [a]*, Charles Augarde [b]

[a] *Department of Geotechnical Engineering, College of Civil Engineering, Tongji University, 1239 Siping Road, Shanghai 200092, China*

[b] *School of Engineering and Computing Sciences, Durham University, South Road, Durham DH1 3LE, UK*

[c] *School of Civil and Resource Engineering, The University of Western Australia, M051, 35 Stirling Highway, Crawley, WA 6009 Australia*

*Corresponding author.

Tel.: +86 21 65985014

Fax: +86 21 65985140

E-mail: yccai@tongji.edu.cn

Abstract

A new meshless sub-region radial point interpolation method (MS-RPIM) is proposed for linear elastic fracture mechanics. The Williams expansions of stress field for mode I/II crack is used as the trial functions in crack tip region, the meshless radial point interpolation is used for the rest of domain, and a mixed variational principle is used for discretisation. In contrast to existing meshless formulations, the present MS-RPIM requires only very few nodes around the crack tip to obtain smooth stress and accurate results and the SIFs can be directly obtained as part of the solution and no additional effort via post-processing.

Keywords: *Crack tip; Meshless; Meshfree; Mixed variational principle; RPIM;*

1. Introduction

The accurate analysis of crack tip fields is of vital importance for the safety assessment and life prediction of cracked engineering structures and materials. Over the past three decades, a wide range of numerical methods have been proposed for fracture modelling. The finite element method (FEM) using quarter-point for standard elements, singular crack tip elements, enriched elements, and hybrid elements [1-5] can be applied for fracture modelling with quite good accuracy. For static cracks, the FEM remains a

dominant numerical tool. However, the method finds difficulties in modelling crack propagation due to the element topology that needs to be updated during crack propagation. More recently, the development of novel numerical methods has attracted much interest for researchers in computational mechanics particularly in the area of meshless methods, which refers to a group of numerical methods requiring no preexisting mesh for the construction of the field approximation. They are particularly suitable for fracture modelling since there is no entanglement problem with large deformations of the mesh requiring updating or remeshing to accommodate the changing geometry of a crack. Some of the prominent methods for crack analysis are the generalized finite element method (GFEM), the extended finite element method (XFEM), smoothed FEM and non-uniform B-spline based FEM [6-8]. These methods together with meshless methods fall generally into the family of partition of unity methods.

Recently, much effort has been directed towards the application of meshless methods to crack problems to overcome the difficulties in traditional numerical methods [9-19]. Despite clear general progress with these methods, there are still some technical issues in their application to fracture problems, for instance, it is often awkward and an expensive task to refine the nodal arrangement near the crack tip in order to increase the solution accuracy, since the stress results tend to be oscillatory near the crack tip. The incorporation of singular functions associated with linear elastic fracture in meshless methods reduces stress oscillations and increases accuracy of stress intensity factor (SIF) significantly [12, 16]. However, introducing such an enriched basis in meshless approximations can lead to ill-conditioning of the global stiffness matrix, and special treatments [12, 17] have to be used to alleviate this problem. Thirdly, many meshless methods employ the *J*-integral or contour integral scheme for the calculation of SIF, which is performed as a post-processing step applied to the stress results, such as in the formulations using the FEM described in [15-19] and partition of unity enriched boundary element method (PU-BEM) [21, 22]. This is unlike the case with the isoparametric FEM or sub-region mixed variational principle based FEM where the SIF can be directly obtained as part of the solution [3-5].

To address the above issues, a new meshless method is proposed in this paper which can be classified as a mixed sub-region radial point interpolation method (MS-RPIM) for analyzing crack tip fields. In this method, Williams expansion of the stress field of mode I/II crack [22] is used as the trial functions in the region near the crack tip,

the meshless RPIM [23, 24] is used for the region far from the crack tip, and a mixed variational principle is used to discretise the governing equations [3]. The present MS-RPIM preserves the advantages of meshless methods where the entanglement of finite element topology is removed, and has further positive features such as a simple formulation for numerical implementation. In contrast to existing meshless formulations for fracture modelling, it has the following advantages. Firstly, only a very few nodes around the crack tip are required to obtain smooth stress results and accurate SIFs. Secondly, solution accuracy and stability are much better than meshless methods using implicit enrichment and it is free from the ill-conditioning problem which affects the global stiffness matrix using explicit enrichment. Finally, the SIFs can be directly obtained as part of the solution; there is no additional effort required to calculate the SIF results via post-processing. The rest of the paper is organized as follows. Section 2 covers the field interpolation used in the MS-RPIM, which is then described in detail in Section 3 including a description of the mixed variational formulation used for discretisation. Finally, Section 4 contains verification examples to show the performance of the method.

2. Point interpolation based on radial basis function

For the convenience of the following discussion, in this section we will briefly describe the field interpolation using the RPIM, used for the stress analysis. The RPIM was originally proposed in [23] and has been recently used for fracture modelling in [16] and [24]. We confine the present study to 2D linear elastic fracture mechanics, with the fundamental field variables being displacements. Consider a problem domain Ω of arbitrary shape discretised by a set of scattered nodes $\{\mathbf{x}_i\}$ as shown in Fig.1. For a given point $\mathbf{x}$ in Ω, there are n distributed nodes in the influence domain Ω_x of point $\mathbf{x}$. Considering one of the two freedoms at a node, the nodal function value is u_i at node $\mathbf{x}_i$. The RPIM is used to construct the approximation function $u(\mathbf{x})$ of the point $\mathbf{x}$ using radial basis functions $B_i(\mathbf{x})$ and polynomial basis functions $P_i(\mathbf{x})$ having m terms

$$u(\mathbf{x}) = \sum_{i=1}^{n} B_i(\mathbf{x}) a_i + \sum_{j=1}^{m} P_j(\mathbf{x}) b_j = \mathbf{B}^{\mathrm{T}}(\mathbf{x})\mathbf{a} + \mathbf{P}^{\mathrm{T}}(\mathbf{x})\mathbf{b} \tag{1}$$

where the vectors are defined as

$$\begin{aligned}
\mathbf{a}^{\mathrm{T}} &= [a_1, a_2, \cdots, a_n] \\
\mathbf{b}^{\mathrm{T}} &= [b_1, b_2, \cdots, b_m] \\
\mathbf{B}^{\mathrm{T}}(\mathbf{x}) &= [B_1(\mathbf{x}), B_2(\mathbf{x}), \cdots, B_n(\mathbf{x})] \\
\mathbf{P}^{\mathrm{T}}(\mathbf{x}) &= [P_1(\mathbf{x}), P_2(\mathbf{x}), \cdots, P_m(\mathbf{x})]
\end{aligned} . \tag{2}$$

By enforcing the interpolation to pass through all n nodes within the influence domain Ω_x, the coefficients a_i and b_i in Eq.(1) can be determined, and the RPIM interpolation can be expressed as

$$u(\mathbf{x}) = \begin{bmatrix} \mathbf{B}^{\mathrm{T}}(\mathbf{x}) & \mathbf{P}^{\mathrm{T}}(\mathbf{x}) \end{bmatrix} \mathbf{G}^{-1} \begin{Bmatrix} \mathbf{u} \\ \mathbf{0} \end{Bmatrix} = \mathbf{\Phi u} = \sum_{i=1}^{n} \phi_i(\mathbf{x}) u_i \tag{3}$$

where $\phi_i(\mathbf{x})$ is the RPIM shape function, $\mathbf{u}$ is the vector of nodal values where

$$\mathbf{u}^{\mathrm{T}} = [u_1, u_2, \cdots, u_n] \tag{4}$$

and $\mathbf{G}$ is

$$\mathbf{G} = \begin{bmatrix} \mathbf{B}_n & \mathbf{P}_m \\ \mathbf{P}_m^{\mathrm{T}} & \mathbf{0} \end{bmatrix} \tag{5}$$

in which

$$\mathbf{B}_n = \begin{bmatrix} B_1(\mathbf{x}_1) & B_2(\mathbf{x}_1) & \cdots & B_n(\mathbf{x}_1) \\ B_1(\mathbf{x}_2) & B_2(\mathbf{x}_2) & \cdots & B_n(\mathbf{x}_2) \\ \vdots & \vdots & \vdots & \vdots \\ B_1(\mathbf{x}_n) & B_2(\mathbf{x}_n) & \cdots & B_n(\mathbf{x}_n) \end{bmatrix}_{m \times m} \tag{6}$$

and

$$\mathbf{P}_m = \begin{bmatrix} P_1(\mathbf{x}_1) & P_2(\mathbf{x}_1) & \cdots & P_m(\mathbf{x}_1) \\ P_1(\mathbf{x}_2) & P_2(\mathbf{x}_2) & \cdots & P_m(\mathbf{x}_2) \\ \vdots & \vdots & \vdots & \vdots \\ P_1(\mathbf{x}_n) & P_2(\mathbf{x}_n) & \cdots & P_m(\mathbf{x}_n) \end{bmatrix}_{n \times m} . \tag{7}$$

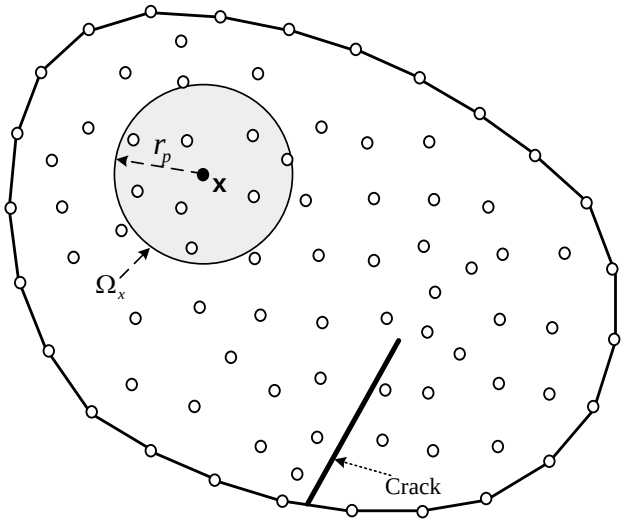

Figure 1. The meshless model for an arbitrary analysis domain

It has been proven in [24] that the RPIM shape functions $\phi_i(\mathbf{x})$ in Eq.(3) possess the Kronecker delta property. Hence, essential boundary conditions in the RPIM method can be directly applied as in the FEM. Here, a linear polynomial basis function

$$\mathbf{P}^{\mathrm{T}}(\mathbf{x}) = [1, x, y] \tag{8}$$

and Gaussian type radial basis function

$$B_i(\mathbf{x}) = \exp\left[-0.31\left(\frac{r_i}{r_p}\right)^2\right] \tag{9}$$

are used in the present study. In Eq. (9), r_p is the radius of the influence domain Ω_x of point $\mathbf{x}$, and r_i is a distance between interpolating point $\mathbf{x}$ and the node $\mathbf{x}_i$ where

$$r_i^2 = (x - x_i)^2 + (y - y_i)^2 \tag{10}$$

To capture the displacement discontinuity due to the existence of crack as shown in Fig. 1, the visibility criterion [12] is used where a point of interest and the nodes supporting that point severed by a crack is not associated in the interpolation. For the determination of the radius r_p at point $\mathbf{x}$, a radius d_i of the support domain for an arbitrary node $\mathbf{x}_i$ in domain Ω is firstly defined as

$$d_i = \alpha \cdot c_i \tag{11}$$

where c_i is set as the distance to the fifth nearest neighbor node near node $\mathbf{x}_i$, α is a coefficient and here $\alpha = 2.7$ for the nodes near the crack and at the boundary, and

$\alpha = 2.0$ for all other nodes. This is due to the fact that when the visibility criterion is used to exclude the nodes cut by the crack, or when an integration point or a sampling point is close to the boundary, less nodes are included as supporting nodes. This may lead to an ill conditioned problem or lower accuracy in the construction of the RPIM interpolation. From the experiences in testing examples, we found that an increase of the coefficient to the value of $\alpha = 2.7$ normally gives results of satisfactory accuracy. Note that we have larger support coefficient for the region where the crack passes through but this is unnecessary for the nodes close to the crack tip since the crack tip region is captured by a sub-region around the crack tip, as will be explained in §3. Assuming that there are total N scattered nodes $\mathbf{x}_k (k = 1, \cdots, N)$ where the given point $\mathbf{x}$ is in the support domain of nodes $\mathbf{x}_k$, the radius r_p of point $\mathbf{x}$ is defined as

$$r_p = \min[d_1, d_2, \cdots, d_N] . \tag{12}$$

3. The meshless sub-region RPIM (MS-RPIM)

In this section, the formulation of the new meshless sub-region radial point interpolation method (MS-RPIM) is described in detail. We start the description of the formulation using a 2D problem domain of arbitrary shape with a preexisting crack as shown in Fig. 1. The key feature of the method is the division of the problem domain into two sub-regions in which different unknowns are solved for. In Fig. 2, the domain is divided into two sub-regions by setting a circle centered on the crack tip with radius *R*. The sub-region bounded by the circle is denoted as V_c, that outside the circle as V_p and the interface between V_c and V_p is marked as S_{pc}. We follow the mixed sub-region method proposed in [3] by taking the stress parameters in V_c and nodal degrees of freedom in V_p as the unknowns. Then the functional of the total potential energy is calculated to include the contribution from V_p denoted as Π_p, the contribution from V_c denoted as Π_c and the energy along the interface S_{pc} denoted as H_{pc}. Note that nodes falling inside V_c are not used for the interpolation in V_p, and are set as invalid nodes when calculating Π_p.

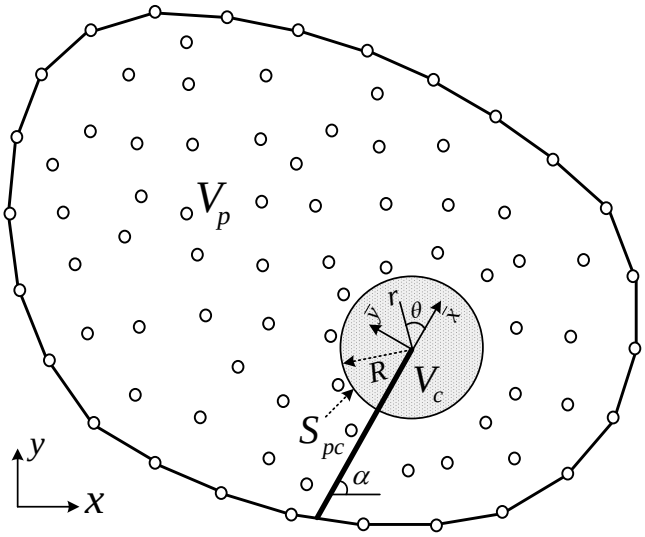

Figure 2. The divisions of the analysis domain into the complementary energy sub-region around the crack tip (shaded area) and the potential energy sub-region distant from the crack.

3.1. The energy term in potential energy sub-region

Here, we solve the problem in solid mechanics with the nodal displacement being unknowns. Denote the nodal displacements in the potential energy sub-region V_p as

$$\mathbf{U} = \left[u_1, v_1, \cdots, u_M, v_M\right]^{\mathrm{T}} \tag{13}$$

where u is the displacement in x direction, v is displacement in the y direction, and M is the total number of nodes in V_p, and the entries of the vector $\left(u_i, v_i\right)$ are the displacements at node i in x and y directions respectively. By using the RPIM interpolation in Eq. (3), the total potential energy in V_p is expressed as

$$\Pi_p = \frac{1}{2}\mathbf{U}^{\mathbf{T}}\mathbf{K}_p\mathbf{U} - \mathbf{U}^{\mathbf{T}}\mathbf{P} \tag{14}$$

where $\mathbf{K}_p$ is the global stiffness matrix of the potential energy sub-region, and $\mathbf{P}$ is the vector of nodal forces.

3.2. The energy term in complementary energy sub-region

We denote the displacement variables in the complementary energy sub-region V_c as

$$\boldsymbol{\beta} = \left[\beta_1, \beta_2, \cdots, \beta_{2m}\right]^{\mathrm{T}} \tag{15}$$

where m is the number of the stress terms. By using Williams expansions of the stress fields near mode I and II crack tips [18], the stress field in the complementrary energy sub-region V_c can be expressed by

$$\boldsymbol{\sigma} = \left[\sigma_{\bar{x}}, \sigma_{\bar{y}}, \tau_{\bar{x}\bar{y}}\right]^{\mathrm{T}} = \mathbf{S}\boldsymbol{\beta} \tag{16}$$

where $\mathbf{S}$ is a vector of the stress functions of the mode I and II crack, i.e.

$$\begin{aligned} \mathbf{S} &= \left[\mathbf{S}^{\mathrm{I}} \quad \mathbf{S}^{\mathrm{II}}\right] \\ \mathbf{S}^{\mathrm{I}} &= \left[\mathbf{S}\mathbf{F}_1^{\mathrm{I}} \quad \mathbf{S}\mathbf{F}_2^{\mathrm{I}} \quad \cdots \quad \mathbf{S}\mathbf{F}_m^{\mathrm{I}}\right] \\ \mathbf{S}^{\mathrm{II}} &= \left[\mathbf{S}\mathbf{F}_1^{\mathrm{II}} \quad \mathbf{S}\mathbf{F}_2^{\mathrm{II}} \quad \cdots \quad \mathbf{S}\mathbf{F}_m^{\mathrm{II}}\right] \end{aligned} \tag{17}$$

and

$$\mathbf{S}\mathbf{F}_k^{\mathrm{I}} = \frac{k}{2}\left(\frac{r}{R}\right)^{\frac{k}{2}-1}\begin{Bmatrix} \left[\frac{k}{2}+2+(-1)^k\right]\cos\left(\frac{k}{2}-1\right)\theta - \left(\frac{k}{2}-1\right)\cos\left(\frac{k}{2}-3\right)\theta \\ -\left[\frac{k}{2}-2+(-1)^k\right]\cos\left(\frac{k}{2}-1\right)\theta + \left(\frac{k}{2}-1\right)\cos\left(\frac{k}{2}-3\right)\theta \\ -\left[\frac{k}{2}+(-1)^k\right]\sin\left(\frac{k}{2}-1\right)\theta + \left(\frac{k}{2}-1\right)\sin\left(\frac{k}{2}-3\right)\theta \end{Bmatrix} \tag{18}$$

$$\mathbf{S}\mathbf{F}_k^{\mathrm{II}} = \frac{k}{2}\left(\frac{r}{R}\right)^{\frac{k}{2}-1}\begin{Bmatrix} \left[\frac{k}{2}+2-(-1)^k\right]\sin\left(\frac{k}{2}-1\right)\theta - \left(\frac{k}{2}-1\right)\sin\left(\frac{k}{2}-3\right)\theta \\ -\left[\frac{k}{2}-2-(-1)^k\right]\sin\left(\frac{k}{2}-1\right)\theta + \left(\frac{k}{2}-1\right)\sin\left(\frac{k}{2}-3\right)\theta \\ \left[\frac{k}{2}-(-1)^k\right]\cos\left(\frac{k}{2}-1\right)\theta - \left(\frac{k}{2}-1\right)\cos\left(\frac{k}{2}-3\right)\theta \end{Bmatrix} \tag{19}$$

where $k = 1, 2, \cdots, m$. Note that r and θ are based on the local coordinate system shown in Fig. 2. Then the potential energy Π_c in the complementary energy sub-region is calculated as

$$\Pi_c = \frac{1}{2}\iint_{V_c} \boldsymbol{\sigma}^{\mathrm{T}}\mathbf{D}^{-1}\boldsymbol{\sigma} t d\bar{x} d\bar{y} = \frac{1}{2}\boldsymbol{\beta}^{\mathrm{T}}\mathbf{F}\boldsymbol{\beta} \tag{20}$$

where $\mathbf{D}$ is the elastic constitutive matrix for plane elastic problemand t is the thickness of the domain. Using the symmetric and antisymmetric terms of mode I and mode II stress expansions, the flexibility matrix in the complementrary energy sub-region can be written as

$$\mathbf{F} = \begin{bmatrix} \mathbf{F}^{\mathrm{I}} & \mathbf{0} \\ \mathbf{0} & \mathbf{F}^{\mathrm{II}} \end{bmatrix} \tag{21}$$

in which

$$\mathbf{F}^{\mathrm{I}} = \iint_{V_c} \left(\mathbf{S}^{\mathrm{I}}\right)^{\mathrm{T}} \mathbf{D}^{-1} \mathbf{S}^{\mathrm{I}} t d\bar{x} d\bar{y} \tag{22}$$

$$\mathbf{F}^{\mathrm{II}} = \iint_{V_c} \left(\mathbf{S}^{\mathrm{II}}\right)^{\mathrm{T}} \mathbf{D}^{-1} \mathbf{S}^{\mathrm{II}} t d\bar{x} d\bar{y} \,. \tag{23}$$

3.3. The energy term along the interface of the sub-regions

The traction vector at any point along the interface S_{pc} shown in Fig. 2 is denoted as $\mathbf{T} = \left[T_x, T_y\right]^{\mathrm{T}}$ and can be calculated as

$$\mathbf{T} = \boldsymbol{\lambda} \mathbf{S} \boldsymbol{\beta} \tag{24}$$

where (r, θ) is the local polar coordinate at that point with respect the crack tip, and $\boldsymbol{\lambda}$ is the transformation matrix with respect to the crack tip given by

$$\boldsymbol{\lambda} = \begin{bmatrix} \cos\alpha\cos\theta & -\sin\alpha\sin\theta & \cos\alpha\sin\theta - \sin\alpha\cos\theta \\ \sin\alpha\cos\theta & \cos\alpha\sin\theta & \sin\alpha\sin\theta - \cos\alpha\cos\theta \end{bmatrix} \quad . \tag{25}$$

Using the displacement at a point along S_{pc}, the displacement inside the sub-region can be interpolated using Eq. (3)

$$\mathbf{u}(r,\theta) = \sum_{i=1}^{n} \varphi_i(\mathbf{x})\ \mathbf{u}_i = \boldsymbol{\Phi} \hat{\mathbf{U}} \,, \tag{26}$$

where $\boldsymbol{\Phi}$ is the matrix of the shape functions of the RPIM, $\hat{\mathbf{U}}$ is the nodal displacement vectors in the potential energy sub-region V_p. The energy term along S_{pc} is then calculated as

$$\mathrm{H}_{pc} = \int_{S_{pc}} \mathbf{T}^{\mathrm{T}} \mathbf{u} t ds = \boldsymbol{\beta}^{\mathrm{T}} \mathbf{H} \hat{\mathbf{U}} \tag{27}$$

where

$$\mathbf{H} = \int_{S_{pc}} \mathbf{S}^{\mathrm{T}} \boldsymbol{\lambda}^{\mathrm{T}} \boldsymbol{\Phi} t ds \quad . \tag{28}$$

3.4. Discretisation of the governing equations based on the mixed variational principle

In this section, we will derive the discretised form of the governing equations for the MS-RPIM method by minimization of the energy functional, as in the standard FEM.

Firstly, we look at the total energy functional which here is the total mixed energy functional denoted as Π, i.e. the summation of the energy terms in Eqs. (14), (20) and (27)

$$\Pi = \Pi_p + \Pi_c + \mathrm{H}_{pc} = \frac{1}{2}\mathbf{U}^{\mathrm{T}}\mathbf{K}_{\mathrm{p}}\mathbf{U} - \mathbf{U}^{\mathrm{T}}\mathbf{P} - \frac{1}{2}\boldsymbol{\beta}^{\mathrm{T}}\mathbf{F}\boldsymbol{\beta} + \boldsymbol{\beta}^{\mathrm{T}}\mathbf{H}\hat{\mathbf{U}}. \tag{29}$$

The stationary condition is applied to Π so that

$$\partial\Pi/\partial\boldsymbol{\beta} = 0, \tag{30}$$

and

$$\partial\Pi/\partial\mathbf{U} = 0. \tag{31}$$

From Eq. (29), we can solve for $\boldsymbol{\beta}$ as

$$\boldsymbol{\beta} = \mathbf{F}^{-1}\mathbf{H}\hat{\mathbf{U}} \ . \tag{32}$$

Substituting Eq. (32) into (29) and considering the stationary condition of Eqs. (30) and (31) gives

$$\mathbf{K}_p\mathbf{U} + \mathbf{H}^{\mathrm{T}}\mathbf{F}^{-1}\mathbf{H}\hat{\mathbf{U}} = \mathbf{P} \ . \tag{33}$$

By taking out the entries of $\mathbf{H}^{\mathrm{T}}\mathbf{F}^{-1}\mathbf{H}$ and adding them to the corresponding nodal stiffness matrix of $\mathbf{K}_p$, the global equation system can be obtained as

$$\mathbf{K}\,\mathbf{U} = \mathbf{P} \tag{34}$$

where $\mathbf{K}$ is the global stiffness matrix by assembling $\mathbf{K}_p$ and $\mathbf{H}^{\mathrm{T}}\mathbf{F}^{-1}\mathbf{H}$ together. Now the nodal displacement $\mathbf{U}$ can be obtained by solving Eq. (34). By substituting $\mathbf{U}$ into Eq. (32), we can obtain the stress coefficients $\boldsymbol{\beta}$ and hence the stress results at any point inside the domain can be evaluated from Eq. (16). Since the stress terms in Eqs. (18) and (19) use the Williams stress expansion as the basic solution, the SIFs for both mode I and II at the crack tip can be directly found as

$$K_{\mathrm{I}} = \sqrt{2\pi R}\,\beta_1 \tag{35}$$

$$K_{\mathrm{II}} = \sqrt{2\pi R}\,\beta_{m+1} \ , \tag{36}$$

where K_{I} and K_{II} are the SIFs for mode I crack and mode II crack respectively. There are a number of advantages using the proposed formulation which are outlined as follows. Firstly, the size of the sub-region around the crack tip can be arbitrarily chosen without

any mesh constraint as with the FEM. Secondly, the SIFs K_I and K_{II} can be directly obtained as part of the solution without calculating the J integral. It is also found that the results obtained are more stable compared with intrinsic or extrinsic enrichments used in meshless methods. Finally, there is no transitional region required as for intrinsic enrichment in [11].

3.5 Numerical integration and implementations

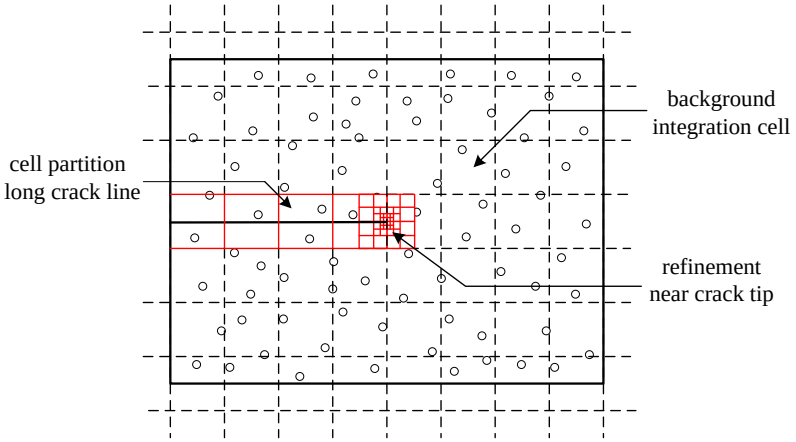

Figure 3. Background integration cells in meshless methods and refinement around the crack tip.

The weak form integration is a key issue in fracture modelling for accurate calculation of crack tip field and hence the extraction of fracture parameters. Many meshless methods requires the use of background integration cell to perform the global weak form integration, such as the Element-free Garlerkin Method (EFGM) and the RPIM. Local weak form based meshless formulation such as the meshless local Petrov-Galerkin (MLPG) method performs integration over nodal support and therefore is regarded as truly meshfree. However the local weak form leads to the loss of symmetry in global stiffness matrix, which is not computational ideal. So here the global weak form integration is adopted using background cells. When background cells are used, it normally involves further geometric operation to consider the crack geometry and its cutting with the analysis domain as shown in Fig. 3. Due to the high energy release rate and stress gradient around a crack tip, refinement of cell near crack tip is also required. As has been in shown [25] the number of integration points required for results of acceptable accuracy is typically about 10 times the total number of nodes, and is heighten for fracture modelling in 2D to 11~12 times for single crack problem in 2D [19]. The integration of the present method is slightly different from that of the EFGM or the original RPIM in that it performs two independent integration over V_p and V_c as shown in Figure 4. In V_p, the integration is performed over each cell which is the same

as the EFGM or RPIM. While in V_c, the integration is performed directly over a circular domain for the complementary energy term in Eqs. (20).

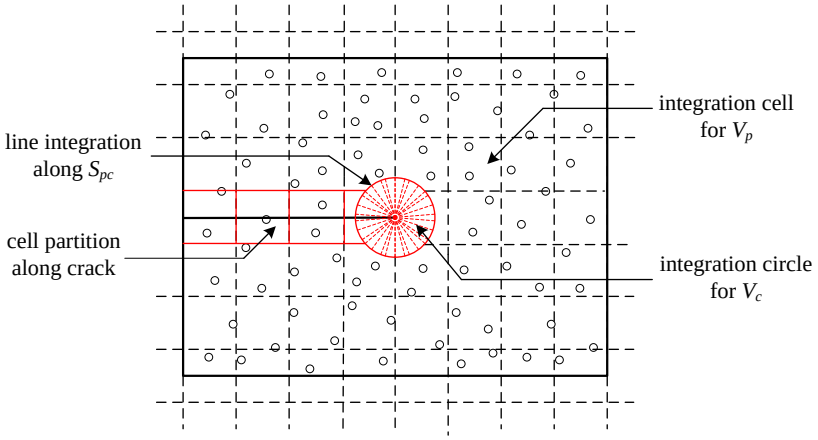

Figure 4. Integration scheme used in the present sub-region RPIM.

Denote the coordinates of crack tip and nodes as $\boldsymbol{x}_{\text{tip}}$ and $\boldsymbol{x}_n$ respectively where the subscript n indicated a node index, and recall that the radius of complementary sub-region is R. The integration and construction of shape functions mainly comprises the following steps.

- Generate the integration cells and nodes through the whole analysis domain.
- Loop over each node and if $\|\boldsymbol{x}_n\text{-}\boldsymbol{x}_{\text{tip}}\| < R$, switch off the nodes in constructing the RPIM shape functions.
- Partition the integration cells with respect to complementary circular domain (as shown in Fig. 4) and adjust the integration cells and points using a certain coordinate mapping scheme.
- Generate integration points inside the circular domain based on polar coordinates.

The integration scheme used for the complementary energy domain is Gaussian integration in both radial and angular directions. Take for example the three-point beam bending problem in§4, the number of integration points in the potential energy and complementary energy sub-regions are 11264 and 900 respectively. The number of nodes used are 962 (including switching off nodes inside V_c), and hence the total integration points is about 12 times the number of nodes, which is similar to the EFGM. In terms of the computational cost in weak form integration, the present method is close to the EFGM or the original RPIM. It should be noted that during crack propagation, V_c will move with the crack tip as it advances, and thus the nodes falling inside V_c in previous calculation steps will be switched on again for constructing the shape function in V_p. Similarly, nodes ahead of crack tip and outside V_c in previous steps may be

switched off. Though these are additional efforts, it does not entail that much cost when a circular domain of V_c is used. Compared with the EFGM or the original RPIM, an additional benefit of the present method is the refinement without partitioning V_c or involving any other geometry operation. In the former two, the cell refinement is like performing another local meshing process, which is undesirable for a meshless method. While in the present method, this can be realized numerically by increasing the divisions of angular and radial integration or by using higher order Gaussian integration scheme. Besides, the refinement here does not affect the shape functions outside V_c, while in the EFGM it will affect nodes in constructing shape functions around the crack tip and also the nodal supports need to be resized with respect to the refine integration points. It is cumbersome to do so in terms of numerical stabilities and convergence.

4. Numerical Examples

Having outlined the formulation of the method, we now present examples to verify performance. In all examples, if not pointed out specifically, the number of stress terms is set as $m = 8$. To accommodate the crack size and node density, the radius of the circle defining V_p is set by the following criterion

$$R = \min\left[0.5l,\ 3c_i\right] \tag{37}$$

where l is the characteristic size of the crack (i.e. equal to the actual length of the crack for a straight crack), c_i is defined in Eq.(11), in which i refers to the index of the node closest to the crack tip.

4.1 Plate with a single edge crack

Consider a rectangular plate with an edge crack of length a located at its mid-height (Fig. 5). The dimensions of the plate are $W = L = 1$ and it is subjected to a uniaxial tensile stress as shown $\sigma = 1$. The problem is solved for the plane stress case with Young's modulus $E = 1000$ and Poisson's ratio $\nu = 0.3$. Note that plate sizes and material parameters here are set regardless of dimensions. For realistic problems, their dimensions should be consistent with each other. The analytical solution for K_I is given in Gdoutos [26] as

$$K_I = \sigma\sqrt{\pi a}\left[1.12 - 0.23\frac{a}{W} + 10.55\left(\frac{a}{W}\right)^2 - 21.72\left(\frac{a}{W}\right)^3 + 30.99\left(\frac{a}{W}\right)^4\right] \tag{38}$$

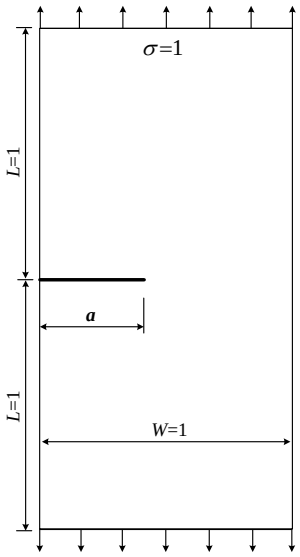

Figure. 5 Analysis domain of an edge crack

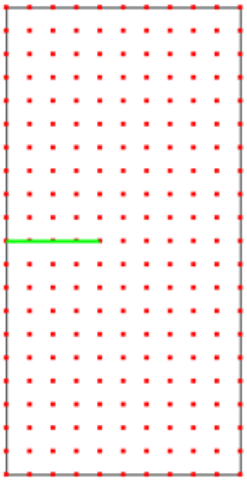

Figure 6. Nodal distributions of the edge-cracked rectangular plate

Results are presented for regular-pattern nodes as shown in Fig. 6. In Table 1, the SIF of the analytical solution, by the MS-RPIM and eRPIM (enriched RPIM by Gu et al. [16]) are compared in terms of the crack length-width ratio $a/W = 0.2 - 0.6$. As the results in Table 1 show, the MS-RPIM leads to stable and accurate results. It is seen that the relative error is less than 1.0% in all cases by using the MS-RPIM. Table 1 indicates that the MS-RPIM solution is much more accurate than the eRPIM solution for sparsely distributed nodes.

Table 1.Comparison of the stress intensity factors for the edge-cracked rectangular plate

a/W	Analytical	eRPIM(231 nodes)		MS-RPIM(231 nodes)	
	K_{I}	K_{I}	Error(%)	K_{I}	Error(%)

0.2	1.09	0.95	-12.8	1.08	-0.57
0.3	1.61	1.39	-13.7	1.62	0.67
0.4	2.36	2.23	-5.5	2.36	0.27
0.5	3.54	3.48	-1.7	3.56	0.49
0.6	5.53	5.63	1.8	5.54	0.24

Fig. 7 shows the sensitivity of the SIF results with respect to the size of complementary energy region and taking the first eight terms of the stress series. The horizontal axis is dimensionless being the ratio R/a and the vertical axis is the relative error of K_{I} with reference to the exact solution. The variation of the SIF by taking different numbers of stress terms is also examined by fixing $R=0.3a$ and the number of nodes but then changing the number of stress terms in Eqs (18) and (19). In Fig. 8, the SIF errors with respect to the exact solution are plotted against the number of terms. It can be seen from Figs. 7 and 8 that an increase of the complementary energy region size, i.e. R, will result in a reduction of the SIF error, and the same effect is seen with an increase in the number of stress terms. However, the influence from the latter does not seem to be as significant as the former. In both figures, the errors tend to converge quickly showing the robustness and satisfactory convergence performance of the proposed method.

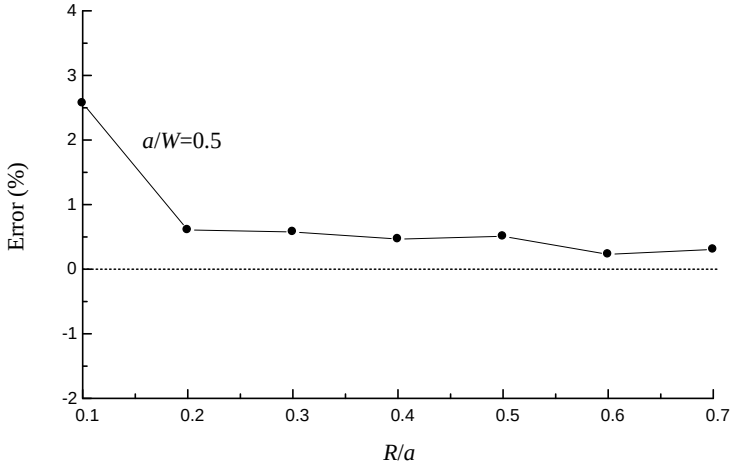

Figure 7. Variation of the SIF errors against various crack tip radius

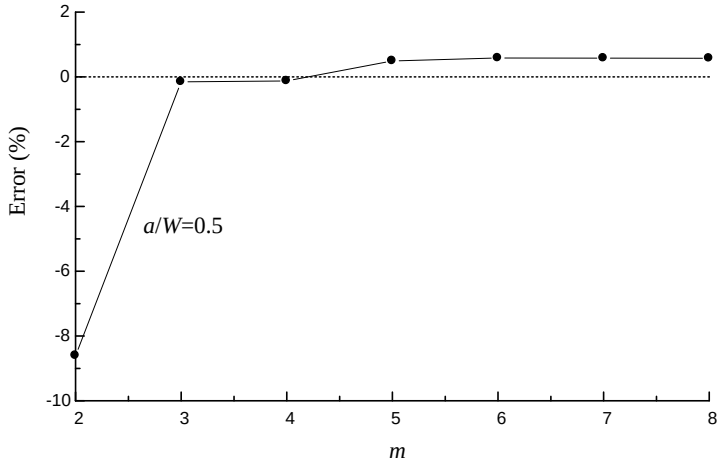

Figure 8. The variation of SIF errors by using different number of stress terms

4.2 A three-point beam bending problem

The problem of a stationary crack in a three-point bend specimen is now considered. The geometry is shown in Fig. 9. The crack is located at the midspan of the beam so that only mode I cracking develops. The dimensions of the specimen are $S=12$ and $W=6$. The load is $F=1$ applied over unit length and unit depth. The discretisation is shown in Fig. 10 and the computed SIFs are compared with the analytical solution obtained by John [27] in Table.2. As it can be seen from the table, the MS-RPIM method shows high solution accuracy for SIFs with the maximum error less than 0.5%.

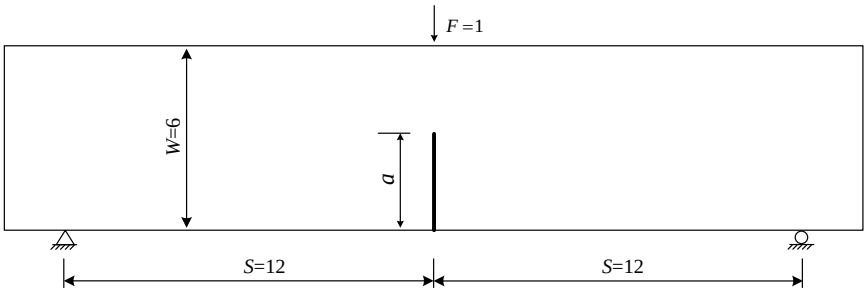

Figure 9. A three-point bending beam

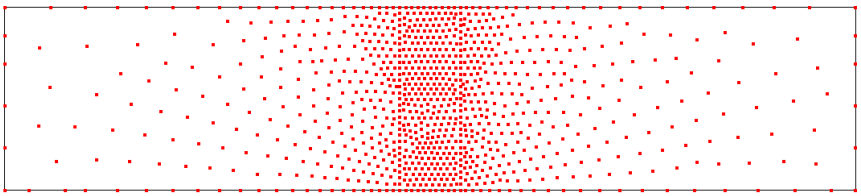

Figure 10. Meshless model of the three-point bending beam

Table 2 SIF results for the three-point beam bending specimen

a/W	K_I (analytical)	K_I (MS-RPIM)	Error(%)
0.3	2.484	2.490	0.23
0.4	3.236	3.236	0.00
0.5	4.348	4.331	-0.38
0.6	6.159	6.148	-0.18

4.3 Plate with a single mode II edge crack

The third problem to verify the method is an edge cracked plate clamped at bottom, and subjected to a far field shear stress $\tau = 1.0$ on the top, as shown in Fig. 11(a). A plane strain state is assumed in this problem. And the discretisation is shown in Fig. 11(b). The reference solution for the stress intensity factors with $a/W = 0.5$ can be found in Fleming *et al*. [12] and these are compared with results from the numerical modelling in Table 3. Once again the MS-RPIM provides very good agreement for K_I and K_{II} values.

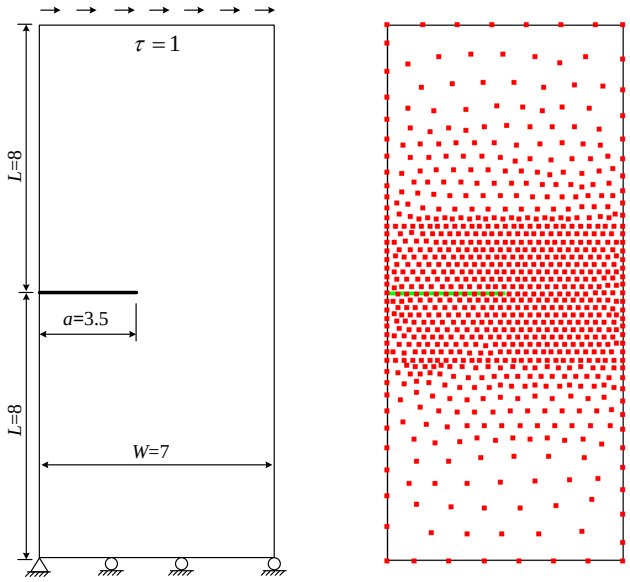

(a) Edge-cracked plate (b) Discrete model

Figure 11. An edge-cracked plate subjected to the shear

Table 3. SIF results for the edge-cracked plate subjected to the shear

	Reference	MS-RPIM	Error(%)
K_I	34.00	34.17	0.50
K_{II}	4.550	4.559	0.20

4.4 Square plate with an inclined central crack

The final verification problem is a square plate with an inclined central crack. The geometry and the node discretisation is shown in Fig. The reference solution for the SIFs for this problem can be found in Murakami [28] and these are compared with the numerical predictions in Table 4, once again showing excellent agreement with the error less than 1%.

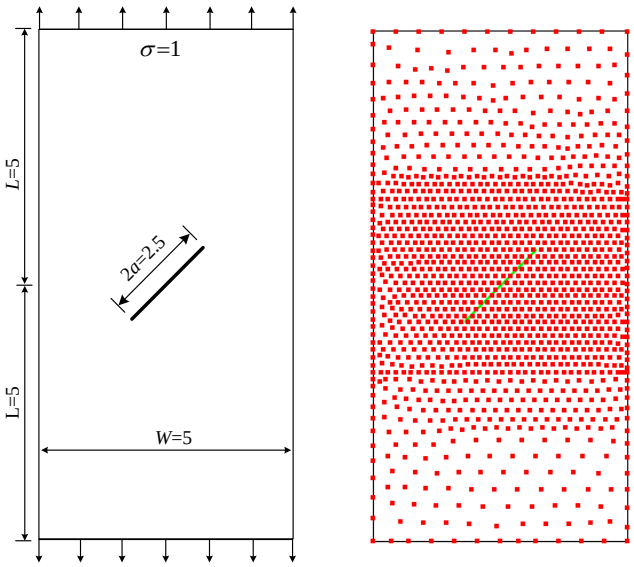

(a) Geometry and boundary conditions (b) Meshless model

Figure 12. Square plate with an inclined central crack

Table 4.SIF results for the inclined central crack

	Reference	MS-RPIM	Error(%)
K_{I}	1.0137	1.0153	0.158
K_{II}	0.9376	0.9380	0.043

5 Conclusions

The accurate modelling of crack tip fields dominated by singular stress field remains a challenging topic computational mechanics. The present paper proposes a mixed sub-region method for fracture modelling combined with the meshless radial point interpolation method. The coefficients for the terms of Williams expansion are used as the unknowns for the sub-region around the crack tip and nodal displacements as unknowns for the sub-region distant to the crack tip. A mixed variational principle is then used to derive the discretised form of the governing equations. The present method

provides an alternative and effective solution for problems of accurate fracture analysis near crack tips. The advantages are that a meshless method is used, i.e. free from meshing and with the capability to deal with moving boundary conditions are preserved while at the same time the SIFs at the crack tip can be directly obtained as part of the solution. Therefore in contrast with the existing meshless formulation for fracture modelling, the present method does not require additional effort in post-processing to calculate the SIFs. It is also elegant in its simple formulation. Several numerical examples demonstrate the effectiveness and robustness of the present MS-RPIM for the analysis of crack tip fields. The test results show that even with sparsely distributed nodes around the crack tip, the accuracy of the SIF remains and the method converges quickly with respect to the sizes of sub-regions and number of stress terms. Despite the above benefits, it can be seen that the integration of the weak form here still requires some efforts and this issue requires further studies which is undergoing by the authors.

Acknowledgements

The authors gratefully acknowledge the support of Nature Science Foundation of China (NSFC 41130751), National Basic Research Program of China (973 Program: 2011CB013800), and Program for Changjiang Scholars and Innovative Research Team in University (PCSIRT, IRT1029), Shanghai Pujiang Talent Program (12PJ1409100).

References

1. Barsoum R. Triangular quarter-point elements as elastic and perfectly-plastic crack tip elements. *International Journal for Numerical Methods in Engineering* 1977; 11:85-98.
2. Kwon YW, Akin JE. Development of a derivative singular element for application to crack propagation problems. *Computers and Structures* 1989; 31:467- 471.
3. Long YQ, Zhao YQ. Calculation of stress intensity factors in plane problems by the sub-region mixed finite element method. *Engineering Software* 1985; 7: 32-35.
4. Benzley SE. Representation of singularities with isoparametric finite elements, *International Journal for Numerical Methods in Engineering* 1974; 8: 537-545.
5. Gifford Jr LN, Hilton PD. Stress intensity factors by enriched finite elements, *Engineering Fracture Mechanics* 1978; 10: 485-496.
6. Strouboulis JT, Babuška I, Copps K. The design and analysis of the generalized finite element method. *Computer Methods in Applied Mechanics and Engineering* 2000; 181: 43-96.
7. Möes N, Dolbow J, Belytschko T. A finite element method for crack growth without remeshing. *International Journal for Numerical Methods in Engineering* 1999; 46: 131–150.

8. De Luycker E, Benson DJ, Belytschko T, Bazilevs Y, Hsu MC. X-FEM in isogeometric analysis for linear fracture mechanics. *International Journal for Numerical Methods in Engineering* 2011; 87: 541-565
9. Vu-Bac N, Nguyen-Xuan H, Chen L, Bordas S, Kerfriden P, Simpson RN, Liu GR, Rabczuk T. A node-based Smoothed eXtended Finite Element Method (NS-XFEM) for fracture analysis. *Computer Modeling in Engineering and Sciences* 2011; 73: 331-355
10. Xu Y, Saigal S, An element free Galerkin formulation for stable crack growth in an elastic solid. *Computer Methods in Applied Mechanics and Engineering* 1998; 154: 331-343
11. Belytschko T, Fleming M. Smoothing, enrichment and contact in the element-free Galerkin method. *Computers and Structures* 1999; 71:173-195
12. Fleming M, Chun YA, Moran B, et al. Enriched element-free Galerkin methods for crack tip fields. *International Journal for Numerical Methods in Engineering* 1997; 40: 1483-1504
13. Zhang Z, Liewa KM, Cheng YM, Lee YY. Analyzing 2D fracture problems with the improved. *Engineering Analysis with Boundary Elements* 2008; 32: 241–250
14. Lee AH, Yoon YC. Numerical prediction of crack propagation by an enhanced element-free Galerkin method. *Nuclear Engineering and Design* 2004; 227:257-271.
15. Duflot M, Huang ND. A meshless method with enriched weight functions for fatigue crack growth. *International Journal for Numerical Methods in Engineering* 2004; 59: 1945-1961.
16. Gu YT, Wang W, Zhang LC, Feng XQ. An enriched radial point interpolation method (e-RPIM) for analysis of crack tip fields. *Engineering Fracture Mechanics* 2011; 78: 175–190.
17. Lu YY, Belytschko T, Gu L. A new implementation of the element free Galerkin method. *Computer Methods in Applied Mechanics and Engineering* 1994; 113: 397-414.
18. Zhuang X, Augarde C and Mathisen K. Fracture modelling using meshless methods and level sets in 3D: framework and modelling. *International Journal for Numerical Methods in Engineering* 2012; 92:969-998. .
19. Zhuang X, Augarde C. and Bordas S. Accurate fracture modelling using meshless methods and level sets: formulation and 2D modelling. *International Journal for Numerical Methods in Engineering* 2011; 86: 249-268.
20. Simpson, RN, Trevelyan, J. A partition of unity enriched dual boundary element method for accurate computations in fracture mechanics. *Computer Methods in Applied Mechanics and Engineering* 2011; 200: 1-10.
21. Simpson, RN, Bordas, SPA, Trevelyan, J, Rabczuk, T. A two-dimensional Isogeometric Boundary Element Method for elastostatic analysis. *Computer Methods in Applied Mechanics and Engineering* 2012; 209-212: 87-100.
22. Williams ML. On the stress distribution at the base of a stationary crack. *Journal of Applied Mechanics* 1957; 24:109-114.
23. Wang JG, Liu GR. A point interpolation meshless method based on radial basis functions. *International Journal for Numerical Methods in Engineering* 2002; 54: 1623-1648.

24. Liu GR, Gu YT. An introduction to meshfree methods and their programming. Berlin: Springer Press; 2005.
25. Dolbow, J. & Belytschko, T. Numerical integration of the Galerkin weak form in meshfree methods. Computational Mechanics, 1999, 23, 219-230
26. Gdoutos EE. Fracture mechanics: an introduction. Kluwer Academic Publishers; 1993.
27. John ES. Wide range stress intensity factor expressions for ASTM E399 standard fracture toughness specimens. *International Journal of Fracture* 1976; 12: 475-476.
28. Murakami Y. Stress Intensity Factors Handbook. New York: Pergamon, 1987.